

Fast degradation of methylene blue with electrospun hierarchical α -Fe₂O₃ nanostructured fibers

Yu Liu · Hongbing Yu · Sihui Zhan ·
Yi Li · Zhenning Lv · Xiaoqing Yang ·
Yunjiang Yu

Received: 30 November 2010 / Accepted: 19 March 2011 / Published online: 13 April 2011
© Springer Science+Business Media, LLC 2011

Abstract The α -Fe₂O₃ fibers have been prepared by electrospinning the corresponding sol–gel precursor, then these fibers were characterized by TGA, SEM, XRD, BET and FT-IR respectively, indicating that the hierarchical α -Fe₂O₃ nanostructured fibers came into being. Photocatalytic degradation of methylene blue (MB) in water was carried out under ultraviolet (UV) light, showing that the fibers had better efficiency for removing MB than other catalysts. And several process parameters have also been studied, which showed that the removal effect of MB was influenced by the process parameters, such as the initial dye concentration, catalyst amounts, inorganic anions, and so on.

Keywords Sol–gel · Photocatalytic · α -Fe₂O₃ fibers · Electrospinning · Methylene blue

1 Introduction

Environmental pollution is a serious challenge to the world. As a typical environmental contaminant, textile dyes and

other industrial dyestuffs are not only aesthetically unpleasant, but are also toxic to some organisms. Degradation of dye effluents has therefore attracted considerable attention during the last two decades [1]. Various methods have been adopted to remove dye pollutants, such as biological treatment, chemical oxidation, electrochemical oxidation, physical techniques, and so on. However, high operating costs and special equipments are needed for traditional physical techniques, which are complicated and inconvenient. Due to the large degree of aromatics present in dye molecules and the stability of modern dyes, conventional biological treatments are ineffective to decolorize the dyes [2–6].

At the present time, advanced oxidation processes (AOPs) are the main emerging routes for the removal of such compounds, which have attracted much attention. Among AOPs, heterogeneous photocatalysis is the most promising technology because of its mild conditions and high efficiency for mineralization. Semiconductor photocatalysis has been shown to be potentially advantageous for removing organic pollutants in wastewater. Many semiconductor oxides, such as TiO₂, WO₃, MnO₂, CeO₂ and ZnO/TiO₂–SiO₂, have been utilized for the photocatalytic degradation of some contaminants [7–11]. Hematite (α -Fe₂O₃) is a stable n-type semiconductor with low bandgap energy of 2.2 eV. It has been applied in photocatalysis, lithium ion battery, gas sensors and magnetic products because it is inexpensive, easily available and non-toxic [12–14].

Presently, polymer-assisted electrospinning offers a simple and cost-effective approach to make one-dimensional (1D) inorganic/semiconductor nanomaterials [15–18]. 1D nanomaterials fabricated by combined sol–gel and electrospinning techniques have such great characteristics as exceptional length, uniform diameter, diverse composition, and high surface, which can be applied in many fields because of their convenience in filtration and recovery [19].

Y. Liu · H. Yu (✉) · S. Zhan (✉) · Z. Lv · X. Yang
College of Environmental Science and Engineering, Nankai University, Tianjin 300071, People's Republic of China
e-mail: sihuizhan@nankai.edu.cn

S. Zhan
e-mail: hongbingyu1130@sina.com

Y. Li
Department of Chemistry, Tianjin University, Tianjin 300072,
People's Republic of China

Y. Yu
Chinese Research Academy of Environmental Sciences, Beijing
100012, People's Republic of China

In this study, α -Fe₂O₃ nanostructured fibers with hierarchical layered structure were obtained by a combination method of sol-gel and electrospinning. Fe₂O₃ fibers are easily available materials of low cost, whose convenience in filtration and recovery makes them suitable for the practical application. Methylene blue (MB) is a typical synthetic cationic dye, whose presence in wastewater may cause the risk of nausea, diarrhea and burn of eye [20]. So MB was selected as a model compound to monitor the photocatalytic activity of the α -Fe₂O₃ fibers. The characteristics of as-prepared fibers were investigated and the photocatalytic degradation of MB in water was evaluated. Furthermore, the effect of several operating parameters, such as the catalyst amounts, initial dye concentrations and inorganic anions, were also researched in detail. The possible photocatalytic kinetics is also brought forward and discussed.

2 Experimental section

2.1 Reagents

MB was obtained from Tianjin Boda Chemical Co. (Tianjin, China). Iron (III) citrate was purchased from Shanghai Chemical Co. (Shanghai, China). Na₂SO₄, NaNO₃ and NaCl were from Tianjin Jiangtian Chemical Co. (Tianjin, China). All reagents were of analytical grade and used without further purification. Deionized and double-distilled water was used throughout this study.

2.2 Characterization

Thermogravimetric analysis (TGA) was performed with a thermogravimetric analyzer (NETZSCH TG 209) at a heating rate of 10 °C min⁻¹ under high pure N₂ flow (20 mL min⁻¹). The surface morphological images of the fibers were obtained by using a scanning electron microscopy (SEM, Shimadzu SS-550). XRD patterns were recorded on a Rigaku D/Max 2500 PC diffractometer with CuK α radiation ($\lambda = 0.154056$ nm). FT-IR spectra were recorded on a Bio-Rad FIS 6000 FTIR spectrometer using the KBr method. BET surface area was determined using a micromeritics tristar 3000.

2.3 The preparation of α -Fe₂O₃ fibers

6.7 g of iron (III) citrate was added in 100 mL double-distilled water and then the mixture was slightly heated and stirred till a homogeneous solution was formed. After being filtrated to remove impurity, the solution was aged at 60 °C in water bath to obtain a viscous sol for further electrospinning. Then the viscous sol was poured into a syringe

(0.7 × 30 TWLB, Jiangxi, China) with a metal needle that was controlled by a syringe pump (Cole-Parmer 74900-05, USA) at a constant flow rate 3.5 mL/h. The metal needle was connected to a high-voltage supply (DW-P503-4ACCD, Tianjin, China), and a piece of stainless steel board was used to collect the gel fibers. All the experiments were carried out at 20 °C, the applied voltage was 25 kV, the distance between the spinneret and the collector was 15 cm. After the collected fibers dried under ambient conditions for several hours, the as-prepared xerogel fibers were annealed at 600 °C for 4 h in air with the heating rate of 10 °C min⁻¹. After being cooled to room temperature, well-crystallined α -Fe₂O₃ nanostructured fibers were obtained. As a comparison, α -Fe₂O₃ nanoparticles were also synthesized using the same procedure but without the further electrospinning.

2.4 Photocatalytic activity

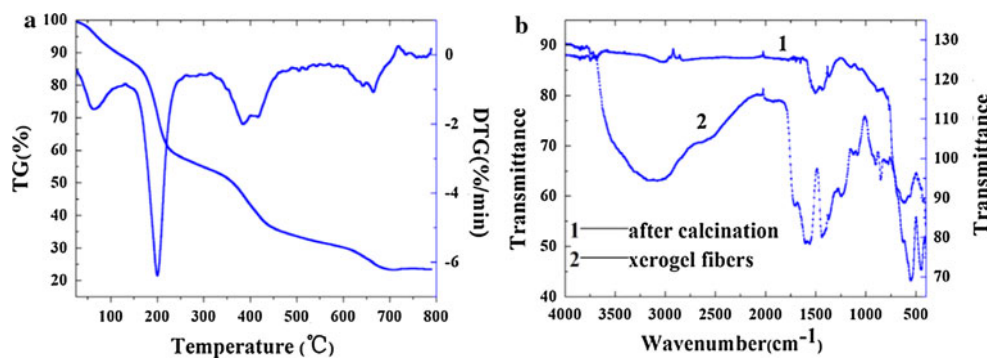
In a typical process, proper amount of catalysts were added in 100 mL of MB solution. A 300 W Hg lamp ($\lambda = 365$ nm, Shanghai Yaming Co., China) was used as UV light source, which was set vertically at a distance of 15 cm above a Pyrex reactor. A cooling jacket was set around the reactor to keep the temperature of reaction solution at 25.0 ± 0.2 °C. During the irradiation, the solution was stirred with a magnetic stirrer. At given time intervals, 3–4 mL of the suspension was sampled and filtered through a Millipore filter (pore size, 0.22 μ m) to remove catalysts. The filtrate was analyzed with a UV-Visible spectrophotometer (Varian, Cary 50 Conc, USA), and the maximum absorbance of MB ($\lambda_{\text{max}} = 664$ nm) was monitored. The degradation efficiency of MB can be calculated by the following equation: Degradation efficiency (%) = $\frac{A_{t=0} - A_t}{A_{t=0}} \times 100\%$. Here A_t is the MB absorbance at 664 nm obtained after various intervals of time (t).

3 Results and discussion

3.1 Characterization of α -Fe₂O₃ fibers

Thermogravimetric analysis (TGA) was performed on the as-spun xerogel fibers to determine the calcination temperature. As illustrated in Fig. 1a, four obvious weight losses appeared in the TG curve. The significant 42% weight losses between 25–175 and 175–240 °C could be attributed to the loss of adsorbed and bound water, and another 34.6% weight loss at 240–570 and 570–680 °C could be caused by the decomposition of citrate. Above 680 °C, there was no further weight loss, which indicated the complete decomposition of the organics. The α -Fe₂O₃

Fig. 1 **a** TG curve of the xerogel fibers; **b** FT-IR spectra of the xerogel fibers and α -Fe₂O₃ fibers



content in the xerogel fibers was 23.4% from the TG analysis, which was in agreement with the content in the commercial ferric citrate (23.5%). This revealed that the aging of the iron citrate solution only resulted in the polymerization of the iron citrate molecules and the formation of spinnable gel.

FT-IR technique was used to track the evolution of xerogel fibers during the heat-treatment. FT-IR spectra of the xerogel fibers and the final products are presented in Fig. 1b. As can be seen in curve 2, in the region of 1,372–1,699 cm⁻¹, the band at 1,601 cm⁻¹ is due to $\nu(\text{C}=\text{O})$, and that at 1,436 cm⁻¹ can be ascribed to $\nu(\text{COO})$. The absorptions appearing between 1,084 and 850 cm⁻¹ can be attributed to the citrate precursor, and the bands below 624 cm⁻¹ are due to $\nu(\text{Fe}-\text{O})$. Curve 1 indicates that the two strong absorption bands at 550 and 445 cm⁻¹ can be attributed to the characteristic lattice vibrations of the hematite phase. And the feeble peak at 3,016 cm⁻¹ can be ascribed to the O–H vibration of adsorbed water on the hematite surfaces [21]. Two small peaks between 1,508 and 1,434 cm⁻¹ could be assigned to the stretching band of C–OH. The feeble peak at 880 cm⁻¹ is caused by C–C stretching [22], which may be due to the remaining carbon. Many studies have demonstrated that doping nonmetallic elements (e.g. nitrogen, carbon, sulfur, iodine, fluorin) into crystal lattice could improve the physicochemical properties and the photocatalytic activities [23–27]. Consequently, the remained carbon element may promote the photoactivity of α -Fe₂O₃ fibers. And how the doped carbon affects the photocatalytic property of the α -Fe₂O₃ fibers will be further researched in the future.

XRD analysis was performed to identify the structure of the α -Fe₂O₃ fibers. Fig. 2 indicates that all diffraction peaks can be indexed to those of hematite (JCPDS:33-0664), showing that the amorphous xerogel fibers completely transformed to well-crystalline hematite fibers after being calcined at 600 °C for 4 h in air. According to the Debye-Scherrer formula, the average diameter of α -Fe₂O₃ particles is estimated to be 27.85 nm. Thus, as-obtained hierarchical α -Fe₂O₃ fibers are nanostructured fibers.

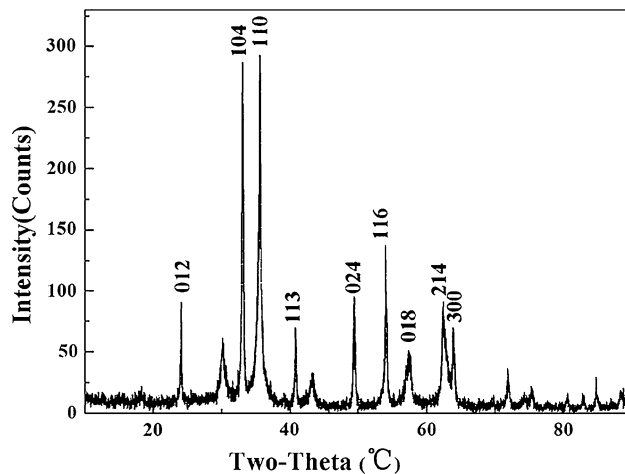


Fig. 2 XRD patterns of the α -Fe₂O₃ fibers calcined at 600 °C for 4 h in air

Fig. 3 shows a typical scanning electron microscopy (SEM) image of the as-prepared α -Fe₂O₃ fibers with a diameter of 0.25–2.5 μm . A view of cross sections (Fig. 3b) indicates that these fibers have unique hierarchical structures, and the uniform layer thickness is only 80 nm. In order to study the formation mechanism of hierarchical structures, the fibers were sampled at different time when being annealed in tubular furnace. Fig. 4. showed SEM images of the α -Fe₂O₃ fibers annealed at 300, 450, 600 °C in the calcining process, and that annealed at 600 °C for 1, 2, and 4 h. As observed from Fig. 4, the fibers were of hollow structure (Fig. 4a, b, d, e) and hierarchical structure (Fig. 4c, f). The hollow structure was consistent with those published by Cairong Gong [28]. After being electrospun and dried in ambient conditions, a rigid outer shell was formed, but the interior of the fiber was still fluid at this stage, and a large amount of water and citrate anions remained in the gel fibers. When the gel fiber was fired, the sol particles diffused to the inner surface of the outer shell with the evaporation of the organic compounds, and thus the tube first came into being. While increasing the heating temperature, citrate anions began to decompose to produce CO₂ and H₂O gases, which went out

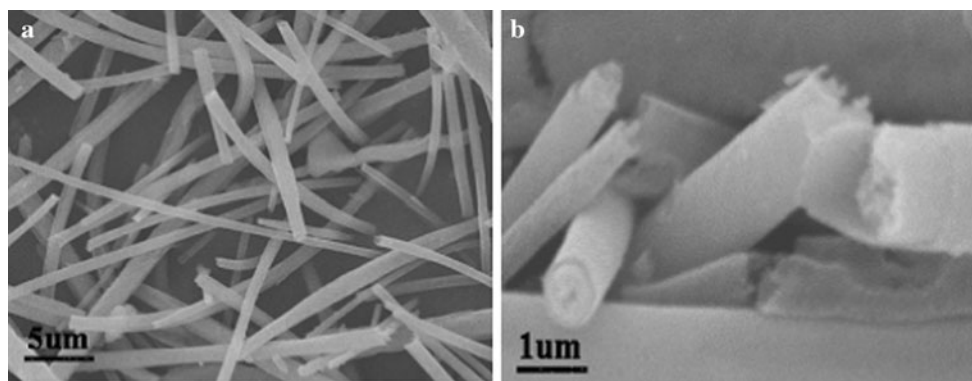


Fig. 3 SEM images of the α -Fe₂O₃ fibers calcined at 600 °C for 4 h in air

of the fibers through the tube, and a crystallized hollow fiber produced [29]. After being dried under ambient conditions for several days, parts of the fibers were of thick rigid outer shells, which helped to form the hollow structure as stated above. Meanwhile, some fibers with more water were of thin xerogel shell. When being annealed, the fluid sol close to the inner surface of the outer shell firstly shrunk and concreted, and the sol particles diffused stepwise to the outer shell. The gradual diffuseness formed interspace between layers and constituted the hierarchical structure of the fibers.

Based on the N₂ adsorption–desorption analysis by a micromeritics tristar 3000, the BET surface area of the fibers is 12 m²/g. However, from the macro point of view, the hierarchical nanostructured fibers still have many active sites and unsaturated surface coordination sites. Therefore, to enhance the photocatalysis by using these fibers as catalysts is reasonable, which has been validated in the following experiments.

3.2 Photocatalysis experiments

3.2.1 Degradation of MB in different systems

The photocatalysis of MB in four different treatment processes was shown in Fig. 5a. Only 59% of the degradation efficiency was observed after 60 min of continuous UV light irradiation without catalyst. However, in the presence of α -Fe₂O₃ fibers with the same UV light irradiation, all of the dye was degraded, showing the excellent photocatalytic activity of α -Fe₂O₃ fibers under UV irradiation. While the suspension was placed in the dark, almost no degradation of MB was observed, suggesting that the degradation of MB was mainly caused by photodegradation rather than adsorption. For comparison, the photocatalysis of self-prepared α -Fe₂O₃ nanoparticles and commercial Fe₂O₃ powder were also evaluated. The results indicated that α -Fe₂O₃ fibers exhibited greater photocatalytic activity

than the others, and the reaction rate decreased with irradiation time. The slower kinetics of dyes degradation is due to the slow reaction of short chain aliphatics with ·OH radicals, and the short life-time of photocatalysts resulted from active sites deactivation by strong by-products deposition [30].

To our knowledge, the detailed mechanism of the photocatalytic decomposition of MB with other catalysts has been discussed previously. According to the studies [31], the color of MB solutions became less intense (hypsochromic effect) when auxochromic groups (methyl or methylamine) were degraded. And for dyes containing auxochromic alkylamine groups, N-dealkylation plays an important role in photocatalytic degradation. Zhang [32] has shown that MB molecules converted to Azure B (trimethylthionine), and further demethylated to Azure A, C and then thionine, while the cleavage of the chromophore ring structure (phenothiazine or thionine) occurred concomitantly. UV–visible spectra of MB changing with reaction time are depicted in Fig. 5b. In our experiment, absorption spectrum was characterized by two main peaks occurred at 664 and 612 nm and other two peaks located at 292 nm and 246 nm, respectively. As observed in Fig. 5b, under UV irradiation, the absorption peak at 664 nm gradually blue-shifted by 26 nm, which was associated with the further demethylation of MB. After reaction for 60 min, the absorbance values diminished and no more specific peaks remained, which indicated clearly that not only decolorization but also degradation of MB took place [33].

3.2.2 Effect of catalyst amounts

A series of experiments were carried out to assess the optimum catalyst loading. Photocatalysis of MB solution (10 mg L⁻¹) was tested with different fibers amounts in the range of 20–100 mg L⁻¹. As seen in Fig. 6, the degradation efficiency of MB increased with increasing catalyst

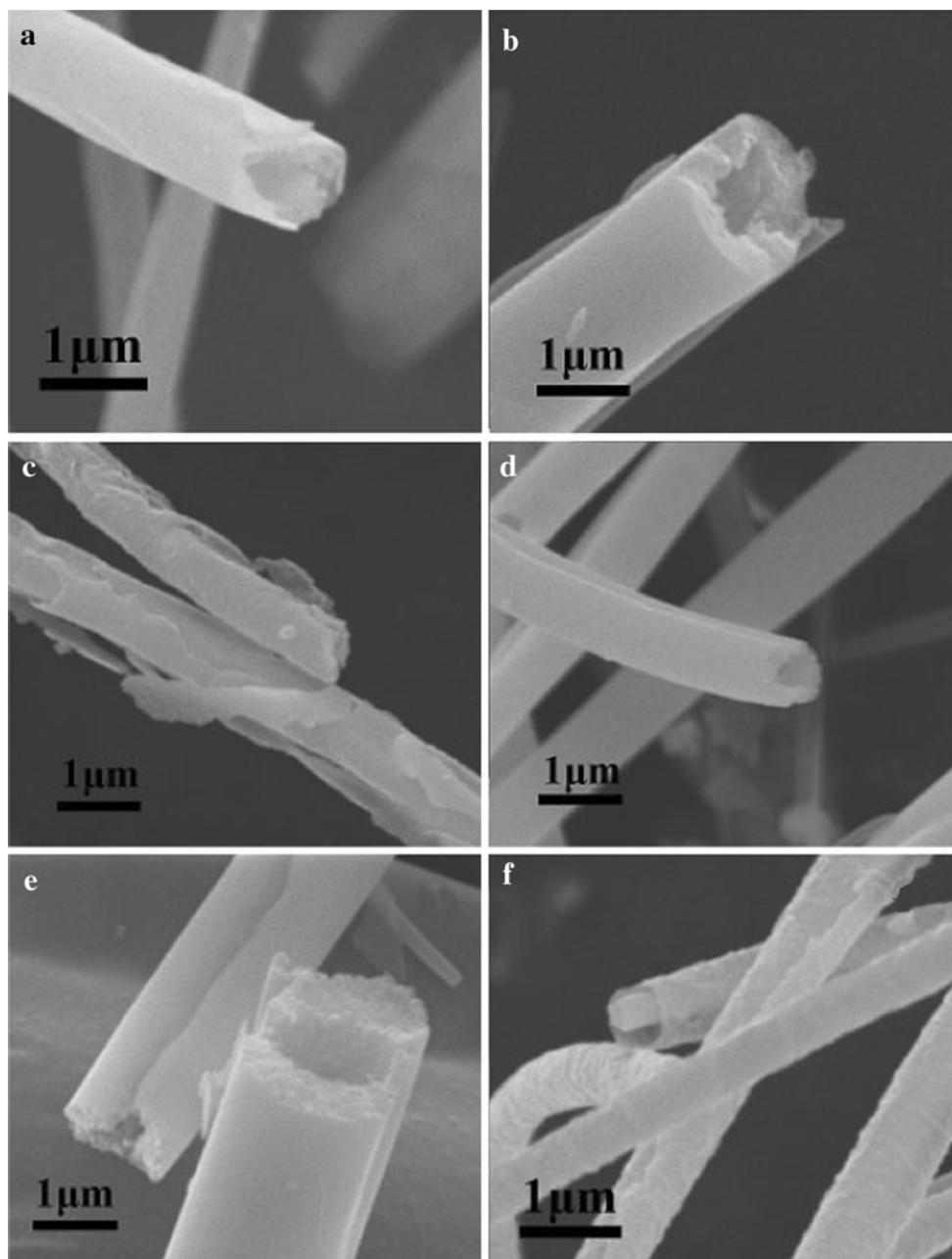


Fig. 4 SEM images of the α - Fe_2O_3 fibers annealed at 300 °C (a), 450 °C (b), 600 °C (c) in the calcining process, and that annealed at 600 °C for 1 h (d), 2 h (e), and 4 h (f)

amount from 20 to 50 mg L^{-1} . This was due to that the increase in catalyst amount to a certain level contributed to the increase in the quantity of photons and dye molecules adsorbed onto the catalyst surface and consequently the degradation efficiency. However, the further increase in catalyst amount to 100 mg L^{-1} led to the decrease of the degradation efficiency. Accordingly, higher amount of catalyst showed a negative effect on the degradation of MB. The availability of active sites increases with the catalyst loading, but the light penetration and the

photoactivated volume of the suspension shrink [34]. And this can also be explained that the increased opacity of the suspension brought light scattering and shielding effect [35]. Moreover, the decrease in the percentage of degradation at higher catalyst amount may due to deactivation of activated molecules by collision with ground state molecules [36]. Hence an optimum amount of catalyst (50 mg L^{-1}) was chosen in this work, in order to avoid unnecessary excess and also ensure total absorption of light photons for efficient photomineralization.

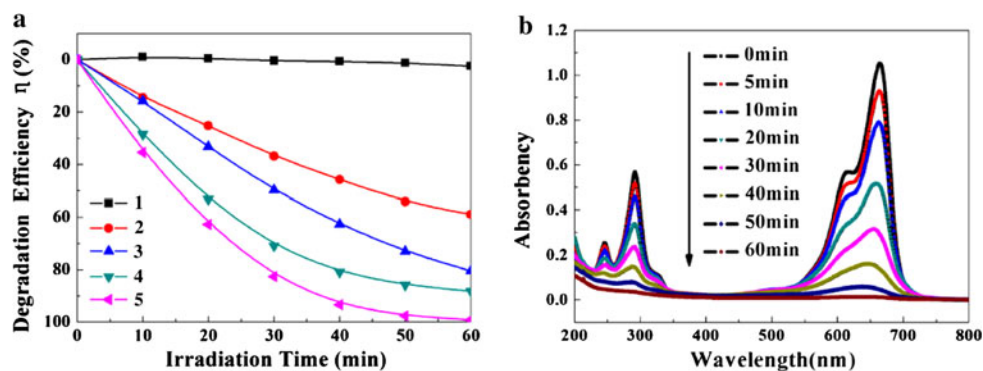


Fig. 5 **a** Comparison of change in degradation efficiency η (%) as a function of irradiation time: (1) α -Fe₂O₃ fibers in the dark (2) Direct UV photolysis without catalyst (3) Commercial α -Fe₂O₃ powder photocatalysis (4) α -Fe₂O₃ nanoparticles photocatalysis (5) α -Fe₂O₃

fibers photocatalysis; **b** UV-vis spectra changes with reaction time in α -Fe₂O₃ fibers photocatalysis. ($[C]_0 = 10 \text{ mg L}^{-1}$, $[\text{catalyst}]_0 = 50 \text{ mg L}^{-1}$, natural pH values (pH = 5.3))

3.2.3 Effect of the initial concentration of dye

Effect of the initial concentration of MB on the degradation efficiency was performed by varying the initial dye concentration from 5 to 30 mg L⁻¹ with constant catalyst loading (50 mg L⁻¹). As shown in Fig. 7, the photodegradation efficiency decreased with the increase in dye concentration. The rate of degradation is related to the formation of hydroxyl free radicals on the catalyst surface and also to the reaction of hydroxyl free radicals with dye molecules. As initial concentration of the dye increased, the probability of ·OH radicals reacting with dye molecules also increased. On the contrary, the active sites on the catalyst surface were replaced and/or covered by dye molecules, then the generation of ·OH radicals would be reduced since there were less active sites available for generation of ·OH radicals. Another important point for this behaviour is that a

high dye concentration would shield the UV light, which makes it difficult for light to trigger the catalysts, thus the formation of hydroxyl free radicals decreases [37].

3.2.4 Effect of co-existing inorganic anions

As we all know, there are large amounts of negative ions in real wastewater produced by textile and dyestuff industries, such as NO₃⁻, SO₄²⁻, Cl⁻ and so on, whose effect on photocatalytic degradation of MB cannot be neglected. Given that the effect of Na⁺ is negligible [38], 0.01 mol L⁻¹ corresponding sodium salts were separately added into the solution when the photocatalytic experiments were carried out. How several typical anions affect the degradation of MB was described in Fig. 8. The presence of NO₃⁻ accelerated the degradation reaction of MB, and Cl⁻ had an inhibitory effect on the degradation

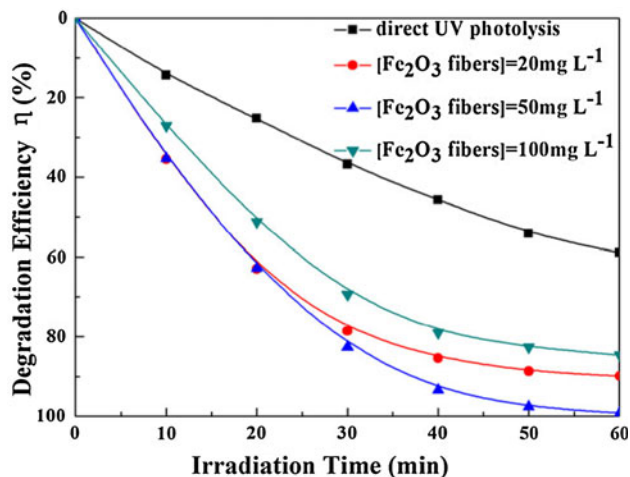


Fig. 6 Catalyst amounts effect on the degradation of MB. $[C]_0 = 10 \text{ mg L}^{-1}$, natural pH values (pH = 5.3)

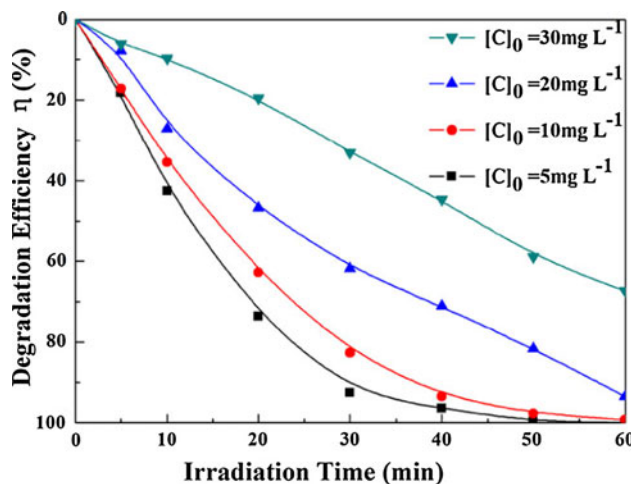


Fig. 7 Influence of the initial MB concentration. $[\alpha\text{-Fe}_2\text{O}_3 \text{ fibers}] = 50 \text{ mg L}^{-1}$, natural pH values (pH = 5.3)

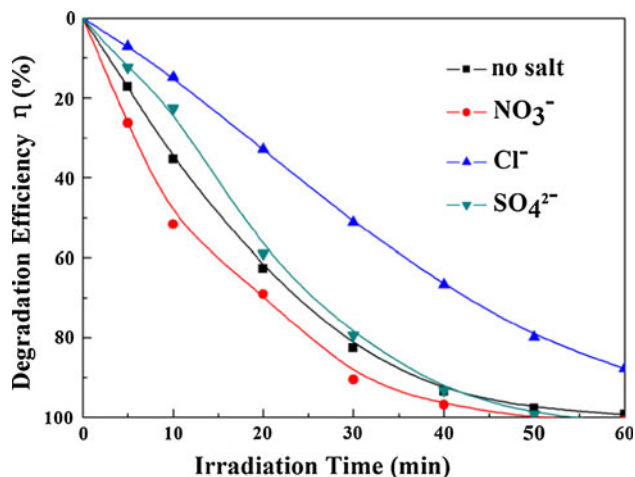
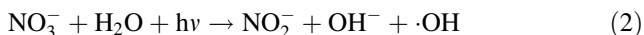


Fig. 8 Influence of co-existing anions on the degradation efficiency of MB. $[C]_0 = 10 \text{ mg L}^{-1}$, $[\alpha\text{-Fe}_2\text{O}_3 \text{ fibers}] = 50 \text{ mg L}^{-1}$, natural pH values (pH = 5.3)

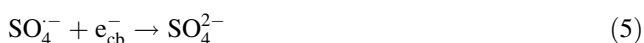
of the dye, whereas retardation effect of SO_4^{2-} was observed.

Chang [39] reported that NO_3^- possessed higher decolorization efficiency of some dyes. The enhanced decomposition in the presence of NO_3^- may link to the direct or indirect formation of hydroxyl radical chemically showed as following reactions [40] (Eqs. (1)–(3)).



Yu studied that the reaction of $\cdot\text{OH}$ with MB molecules resulted in $-\text{CH}_3$ elimination, N–H formation, $\text{C}_{\text{Ar}}-\text{N}$ scission and then the MB central ring breakup [41]. N. Daneshvar and G.A. Epling confirmed that Cl^- was an effective hydroxyl radical scavenging agent [42, 43]. This result is also consistent with those published by M. Abdullah who reported a strong inhibiting effect of chloride ions [38]. This is also why we choose iron citrate rather than iron chloride as precursor when preparing the catalyst.

I.K. Konstantinou has reviewed that the prolonged dye removal can be explained as the reaction of positive holes and $\cdot\text{OH}$ with SO_4^{2-} , which act as h^+ and $\cdot\text{OH}$ scavengers (Eqs. (4) and (5)) [44].



Whereas B. Neppolian reported that sulphate radical anion ($\text{SO}_4^{\cdot-}$) was a powerful oxidant which could trap the photogenerated electrons and generate $\cdot\text{OH}$ as follows (Eqs. (6) and (7)).

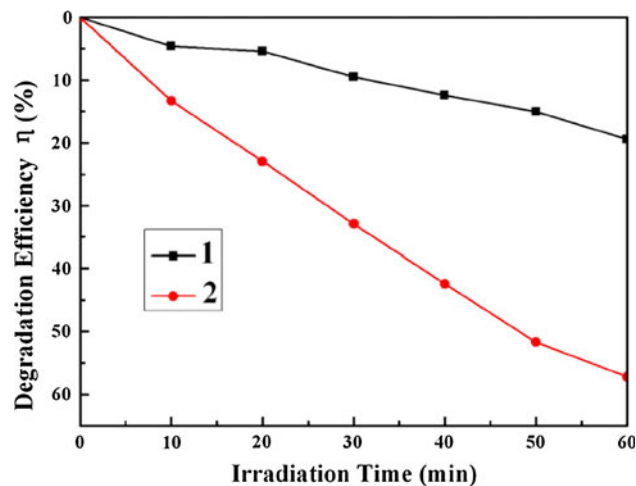
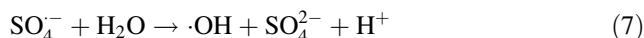


Fig. 9 Comparison of change in degradation efficiency η (%) as a function of irradiation time: (1) Direct UV photolysis without catalyst (2) $\alpha\text{-Fe}_2\text{O}_3$ fibers photocatalysis. (UV intensity = $137 \mu\text{W cm}^{-2}$, $[C]_0 = 10 \text{ mg L}^{-1}$, $[\text{catalyst}]_0 = 50 \text{ mg L}^{-1}$, natural pH values (pH = 5.3))



Therefore, according to Eqs.(4)–(7), SO_4^{2-} can play a dual role: as a strong oxidant and as a $\cdot\text{OH}$ scavenger. Although the reactivity of $\text{SO}_4^{\cdot-}$ may be considered, it is not as reactive as h^+ and $\cdot\text{OH}$ [34, 45]. Thus, the observed retardation effect can be rationalized in terms of strong adsorption of the SO_4^{2-} on the catalysts surfaces [46].

3.2.5 Effect of UV intensity

In order to reduce the effect of UV-light, a UV short-cut filter was used to keep the UV intensity reaching the solution being $137 \mu\text{W cm}^{-2}$. The photocatalysis of MB in this condition was shown in Fig. 9. Only 19% of the degradation efficiency was observed after 60 min of continuous UV light irradiation without catalyst. However, in the presence of $\alpha\text{-Fe}_2\text{O}_3$ fibers under the same UV light, the degradation efficiency of the dye reached 57%, showing the excellent photocatalytic activity of $\alpha\text{-Fe}_2\text{O}_3$ fibers under UV irradiation.

4 Conclusions

$\alpha\text{-Fe}_2\text{O}_3$ nanostructured fibers with unique hierarchical structures have been prepared by combined sol-gel with electrospinning technique. What's more, Fe_2O_3 fibers are easily available materials of low cost, whose convenience in filtration and recovery makes them suitable for the practical application. The photocatalytic degradation of

MB verified the photocatalytic properties of the hierarchical α -Fe₂O₃ fibers. It was found that the initial dye concentration, the photocatalysts amounts, and the co-existing anions had great influence on the photodegradation of MB. The better understanding of these operative conditions could give opportunities for their application in the treatment of dye effluents and other environmental organic contaminants.

Acknowledgments The authors gratefully acknowledge the financial support of National Natural Science Foundation of China (20907022, 21003094), Doctoral Program of Higher Education of China (200800551003, 20100032120066) and Special Projects of Environmental Protection (2009ZX07208, 200909101). Professor Christine Norman is gratefully appreciated for her help in manuscript preparation.

References

- Baldrian P, Merhautová V, Gabriel J, Nerud F, Stopka P, Hrubý M, Beneš MJ (2006) *Appl Catal B* 66:258–264
- Van der Zee FP, Villaverde S (2005) *Water Res* 39:1425–1440
- Rocher V, Siaugue JM, Cabuil V, Bee A (2008) *Water Res* 42:1290–1298
- Vanhulle S, Trovaslet M, Enaud E, Lucas M, Taghavi S, Van der Lelie D, Van Aken B, Foret M, Onderwater RCA, Wesenberg D, Agathos SN, Schneider YJ, Corbisier AM (2008) *Environ Sci Technol* 42:584–589
- Liu CH, Wu JS, Chiu HC, Suen SY, Chu KH (2007) *Water Res* 41:1491–1500
- Prigione V, Tigrini V, Pezzella C, Anastasi A, Sannia G, Cristina Varese G (2008) *Water Res* 42:2911–2920
- Zhao D, Chen CC, Wang YF, Ma WH, Zhao JC, Rajh T, Zang L (2008) *Environ Sci Technol* 42:308–314
- Sayama K, Hayashi H, Arai T, Yanagida M, Gunji T, Sugihara H (2010) *Appl Catal B* 94:150–157
- Jarrige J, Vervisch P (2009) *Appl Catal B* 90:74–82
- Song S, Xu LJ, He ZQ, Chen JM, Xiao XZ, Yan B (2007) *Environ Sci Technol* 41:5846–5853
- Ismail Adel A (2008) *Appl Catal B* 85:33–39
- Eggleston CM, Shankle AJA, Moyer AJ, Cesar I, Grätzel M (2009) *Aquat Sci* 71:151–159
- Zeng SY, Tang KB, Li TW, Liang ZH, Wang D, Wang YK, Qi YX, Zhou WW (2008) *J Phys Chem C* 112:4836–4843
- Fang XL, Chen C, Jin MS, Kuang Q, Xie ZX, Xie SY, Huang RB, Zheng LS (2009) *J Mater Chem* 19:6154–6160
- Jaworek A, Krupa A, Lackowski M, Sobczyk AT, Czech T, Ramakrishna S, Sundarrajan S, Pliszka D (2009) *J Electroanal Chem* 67:435–438
- Lamastra FR, Bianco A, Meriggi A, Montesperelli G, Nanni F, Gusmano G (2008) *Chem Eng J* 145:169–175
- Wu H, Pan W (2006) *J Am Ceram Soc* 89:699–701
- Zhan SH, Chen DR, Jiao XL, Tao CH (2006) *J Phys Chem B* 110:11199–11204
- Formo E, Lee E, Campbell D, Xia YN (2008) *Nano Lett* 8:668–672
- El-Sharkawy EA, Soliman AY, Al-Amer KM (2007) *J Colloid Interf Sci* 310:498–508
- Chen DH, Chen DR, Jiao XL, Zhao YT (2003) *J Mater Chem* 13:2266–2270
- Li X, Yu X, He JH, Xu Z (2009) *J Phys Chem C* 113:2837–2845
- Kisch H, Sakthivel S, Janczarek M, Mitoraj D (2007) *J Phys Chem C* 111:11445–11449
- Liu HM, Imanishi A, Nakato Y (2007) *J Phys Chem C* 111:603–610
- Yu JC, Ho WK, Yu JG, Yip HY, Wong PK, Zhao JC (2005) *Environ Sci Technol* 39:1175–1179
- Hong XT, Wang ZP, Cai WM, Lu F, Zhang J, Yang YZ, Ma N, Liu YJ (2005) *Chem Mater* 17:1548–1552
- Hattori A, Tada H (2001) *J Sol-Gel Sci Technol* 22:47–52
- Gong CR, Chen DR, Jiao XL, Wang QL (2002) *J Mater Chem* 12:1844–1847
- Aizawa M, Nakagawa Y, Nosaka Y, Fujii N, Miyama H (1990) *J Non-Cryst Solids* 124:112–115
- Walling C (1975) *Acc Chem Res* 8:125–131
- Mohammad T, Morrison H (2000) *Photochem Photobiol* 71:369–381
- Zhang TY, Oyama T, Aoshima A, Hidaka H, Zhao JC, Serpone N (2001) *J Photochem Photobiol A* 140:163–172
- Sharma SD, Saini KK, Kant C, Sharma CP, Jain SC (2008) *Appl Catal B* 84:233–240
- Erdemoğlu S, Aksu SK, Sayılkan F, İzgi B, Asiltürk M, Sayılkan H, Frimmel F, Güçer Ş (2008) *J Hazard Mater* 155:469–476
- Huang ML, Xu CF, Wu ZB, Huang YF, Lin JM, Wu JH (2008) *Dyes Pigm* 77:327–334
- Neppolian B, Choi HC, Sakthivel S, Arabindoo B, Murugesan V (2002) *Chemosphere* 46:1173–1181
- Liu CC, Hsieh YH, Lai PF, Li CH, Kao CL (2006) *Dyes Pigm* 68:191–195
- Abdullah M, Low GKC, Matthews RW (1990) *J Phys Chem* 94:6820–6825
- Chang JS, Kuo TS (2000) *Bioresour Technol* 75:107–111
- Zhu HY, Jiang R, Xiao L, Chang Y, Guan YJ, Li XD, Zeng GM (2009) *J Hazard Mater* 169:933–940
- Yu ZQ, Chuang SSC (2008) *Appl Catal B* 83:277–285
- Daneshvar N, Salari D, Khataee AR (2003) *J Photochem Photobiol A* 157:111–116
- Epling GA, Lin C (2002) *Chemosphere* 46:937–944
- Konstantinou IK, Albanis TA (2004) *Appl Catal B* 49:1–14
- Hu C, Yu JC, Hao Z, Wong PK (2003) *Appl Catal B* 46:35–47
- Sökmen M, Özkan A (2002) *J Photochem Photobiol A* 147:77–81